Research Article | Vol. 34, No. 2 / 26 Jan 2026 / Optics Express 1617

Optics EXPRESS

Supercontinuum generation in 1-decanol

NATHAN G. DROUILLARD,[1,*] JACOB A. STEPHEN,[1] CHATHURANGANI JAYALATH ARACHCHIGE,[1] JEET SHANNIGRAHI,[2] AND T. J. HAMMOND[1]

[1]Dept. of Physics, University of Windsor, Windsor ON N9B 3P4, Canada
[2]Dept. of Physics and Astronomy, University of British Columbia, Vancouver BC V6T 1Z1, Canada
[*]droui116@uwindsor.ca

Abstract: Although solids have been recently used in ultrafast experiments for spectral broadening due to their relatively high nonlinearity, their sensitivity to damage limits their long-term stability. Liquids are a possible alternative to solids as a nonlinear medium because of their comparable nonlinearity and resistance to permanent damage. We generate a supercontinuum in 1-decanol that spans from approximately 450 nm to 950 nm. We measure the nonlinear index of refraction of 1-decanol and find a significant n_4 contribution. This contribution leads to a nonlinearity comparable to CS_2 (a frequent reference for nonlinear optics) in high-intensity regimes while being significantly less volatile and toxic. We find this supercontinuum spectrum to be stable for at least 30 minutes.

1. Introduction

Ultrashort and few-cycle laser pulses require supercontinuum (SC) spectra spanning more than an octave of bandwidth [1]. Few-cycle laser pulses offer a route of coherent control on a femtosecond (1 fs = 1×10^{-15}s) timescale, driving experiments in strong-field physics, high-harmonic generation, and attosecond science [2–6]. SC generation has been successfully achieved in gases [7–9] and in solids [10–12] with spectra spanning more than an octave. More recently, SC generation in liquids has been a growing area of study, particularly in hollow-core fibres [13] and liquid-core photonic-crystal fibres (PCFs) [14]. In bulk media, such broad spectra are often referred to as white light continua, as demonstrated for example by Manzoni et al. [15].

Liquids are favourable media for nonlinear optics due to their high density, high nonlinearity, and good power stability [16]. Ethanol has successfully generated SC in a PCF [17], although its volatility and low boiling point limit its stability [18]. Among the commonly used and effective liquids for SC generation are chloroform ($CHCl_3$) [19], carbon disulfide (CS_2) [20], toluene (C_7H_8) [14], and benzene (C_6H_6) [13]. A significant drawback of using these four liquids is that they are all highly toxic [21–24]. Due to the volatility and associated health risks with these organic solvents, we began studying high boiling point organic alcohols instead. The MAK ("maximale Arbeitsplatz-Konzentration" : maximum workplace concentration) [25] of 1-decanol is reportedly 10 mL/m^3 with no reported carcinogenicity [26], compared to a value of 5 mL/m^3 for carbon disulfide [27], 0.5 mL/m^3 for chloroform [28], 5 mL/m^3 for benzene [29], and 50 mL/m^3 for toluene [30] (but toluene vapours are known to be harmful in comparison to 1-decanol [31]).

We have previously studied the effects of 1-decanol on intense femtosecond pulses and found that its high boiling point (231.85 °C) [32] leads to stable pulse compression by a factor of three that is readily achievable [33]. In this paper, we further explore the nonlinear optical properties of 1-decanol, demonstrating significant contributions from higher-order nonlinearities while generating white light continuum (WLC) spanning from 450 nm to 950 nm. We use the z-scan method to extract the Kerr nonlinearity in 1-decanol and find that it is significantly intensity dependent, which allows us to characterize the next order n_4 nonlinearity up to 10^{15}

#581427 https://doi.org/10.1364/OE.581427
Journal © 2026 Received 10 Oct 2025; revised 3 Dec 2025; accepted 19 Dec 2025; published 13 Jan 2026

Optics EXPRESS

W/m ^{2}. At higher intensities, we find that this higher-order contribution leads to a spatial optical soliton that dramatically increases the bandwidth by increasing the interaction region of high intensity without power loss. In addition, we demonstrate the stability of the WLC spectrum over 30 minutes, supporting long-term and repeated use of 1-decanol as a nonlinear medium for strong-field experiments.

2. Methods

As shown in Fig. 1(a), we use a Ti:Sapphire laser that produces 100 fs, 1.5 mJ pulses centered at 785 nm with 1 kHz repetition rate. The beam passes through a half-wave plate ($\lambda/2$) and a polarizer (Pol.) to control the power. A 200 mm focal length lens focuses the beam into the 1 cm cuvette of 1-decanol, which sits on an automated translation stage (Thorlabs PT1-Z8). The beam waist is measured to be 26 µm at the focus, giving a free-space Rayleigh range of $z_0 \approx 2.7$ mm and $z_R \approx 4$ mm inside the liquid [34]. When measuring the spectrum as a function of radial position, the spectrometer is placed 45 cm after the 200 cm focusing lens with no second lens after the cuvette so the beam is not focused into the slit of the spectrometer; instead, the spectrometer is scanned through the beam radially.

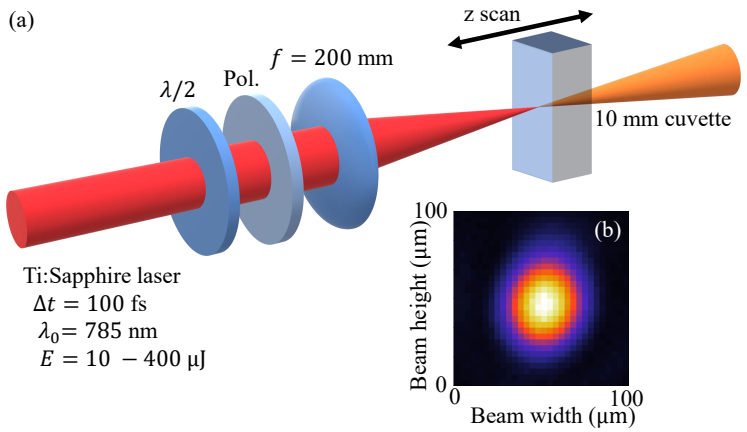

Fig. 1. (a) Experimental setup used for supercontinuum generation in 1-decanol. The beam travels from left to right passing through a half-wave plate ($\lambda/2$), followed by a polarizer (Pol.), a 200 mm focal length lens, and finally into a cuvette which sits on an automated translation stage. Not shown is the spectrometer that measures the spectrum of the output beam. (b) An image of the radial beam profile is shown.

In both the radial and axial cases, the data is taken using 3 wavelength filters and stitched together during data analysis to increase the dynamic range and to better resolve both the visible and infrared portions, which are relatively weaker in intensity compared to the central wavelength. To this end, the spectrum is measured with no filter in order to resolve the spectrum from 740-800 nm. Next, the same measurement is made using a visible filter (335-610 nm)(Thorlabs FGB37M), and two infrared (IR) filters (800-850 nm and 850 nm long-pass). Normalization is required to account for different spectrometer integration times and different degrees of beam attenuation before the spectrometer.

Filter transmission is corrected using measured transmission curves for each visible and IR filter. Because each filter isolates a defined passband, we retain only that wavelength region and stitch it to the unfiltered and visible spectra by matching their overlap in amplitude. A Savitzky–Golay filter is applied for mild smoothing before plotting. Our data and code are available in Ref. [35].

Optics EXPRESS

3. Results and discussion

3.1. Measuring the nonlinear index of refraction

We measure the nonlinear index of refraction of 1-decanol with the closed-aperture Z-scan technique [36]. The sample is translated through the focal region of the beam, and the on-axis transmittance through a small aperture is recorded as a function of position. The nonlinear phase shift accrued by the beam due to self focusing depends on the Kerr coefficient n_2, the peak intensity I_0, and the propagation distance within the material. Self-focusing modifies the beam divergence on either side of the focus, producing the characteristic curve shown in Fig. 2(a).

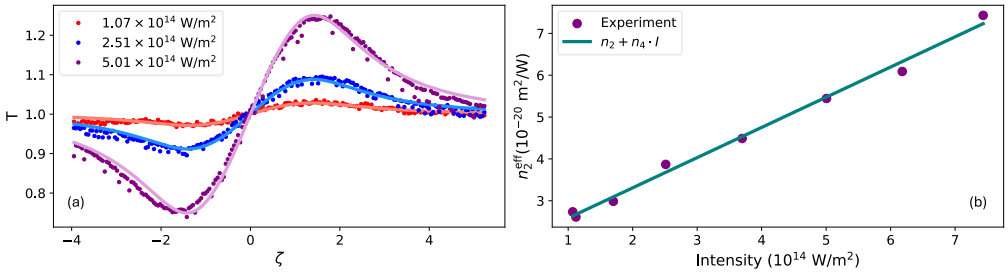

Fig. 2. (a) Low-intensity regime. The points are measured data while the solid lines are the corresponding curve fits. T is the transmittance, which is a function of normalized length $\zeta = z/z_0$ where z is the direction of beam propagation and z_0 is the Rayleigh range [33]. (b) Effective nonlinear index values $n_2(I_0)$ extracted from individual low-intensity Z-scan fits such as (a), plotted as a function of input intensity.

The close-aperture transmission is defined by the function,

$$T = 1 + \Delta\Phi F(\zeta, l) \tag{1}$$

where $\Delta\Phi = (2\pi/\lambda)n_2^{\text{eff}} z_0 I_0$ is the self-focusing-induced nonlinear phase shift, λ is the laser central wavelength, n_2^{eff} is the effective nonlinear index coefficient [37], z_0 is the (free space) Rayleigh range, and I_0 is the peak intensity. The effective nonlinear index coefficient is defined by the third order (Kerr) nonlinear coefficient n_2 and the fifth-order coefficient n_4, where $n_2^{\text{eff}} = n_2 + n_4 I$. The characteristic Z-scan function for a thick sample is defined by the function,

$$F(\zeta, l) = \frac{1}{4} \ln\left(\frac{\left[(\zeta + l/2)^2 + 1\right]\left[(\zeta - l/2)^2 + 9\right]}{\left[(\zeta - l/2)^2 + 1\right]\left[(\zeta + l/2)^2 + 9\right]} \right), \tag{2}$$

where the parameters $\zeta = z/z_0$ and $l = L/z_0$ scale the scanning length and the cuvette length, respectively. The effective nonlinear index coefficient, n_2^{eff}, is then extracted from the fit of the Z-scan curves.

We use a refractive index of 1.43 [38], which agrees with our previous measurement of the dispersion and refractive index of 1-decanol [34]. Since n_2^{eff} is extracted only from the low-intensity Z-scan data, where the spectrum does not broaden significantly, Eq. (1) depends only on the refractive index at the pump wavelength. Given that the refractive index of 1-decanol varies by <1% throughout the measured range, treating it as wavelength-independent is justified for this analysis.

Figure 2(a) shows the low-intensity regime where we do not see SC, but the data follows a typical Z-scan shape. By fitting the data to Eq. (1), we determine the effective nonlinearity, $n_2^{\text{eff}}(I_0)$, at each intensity. The effective nonlinearity increases linearly as a function of peak intensity in the low-intensity regime. Therefore, Fig. 2(b) illustrates how in the low-intensity regime, we can

Optics EXPRESS

fit n_2^{eff} as a function of intensity to calculate $n_4 = 7.22 \times 10^{-35}$ m^4/W^2. Extrapolating the linear fit to the y-intercept yields the Kerr coefficient $n_2 = 1.87 \times 10^{-20}$ m^2/W.

Compared to some values of n_2 reported in the literature for CS_2, a commonly used medium for supercontinuum generation, the n_2 of 1-decanol is lower by approximately an order of magnitude ($n_2(CS_2) \approx 2.8 \times 10^{-19}$ m^2/W) [39,40]. However, n_4 for CS_2 is reportedly $n_4 = -2 \times 10^{-35}$ m^4/W^2 at 800 nm [41], where the change of sign is related to the location of the third harmonic compared to the absorption bands of the medium [42]. Therefore, we have shown that 1-decanol exhibits a degree of optical nonlinearity on par with CS_2 without a high degree of toxicity. In fact, using the cited values, the effective nonlinear index of 1-decanol exceeds that of CS_2 above 2.8×10^{15} W/m^2, which is the regime where we report SC generation.

Aside from our previous measurement [33], there are very few known measurements of the optical nonlinearity of 1-decanol. Ho et al. report $n_2 = 10.9 \times 10^{-20}$ m^2/W, measured using a picosecond (ps) laser centered at 1.06 μm [43], while Kuzyk and Dirk [36] obtain $n_2 \approx 622 \times 10^{-20}$ m^2/W using a nanosecond (ns) laser centered at 1064 nm by converting the Kerr constant B_0 reported in Ref. [44]. Table 1 summarizes all known reports of n_2 for 1-decanol. It should be noted that the nonlinear phase imparted by the cuvette is small compared to that of the liquid, due to the thickness of the cuvette walls being much smaller than that of the liquid. Nevertheless, we do include the nonlinearity of the cuvette in our model [45].

Table 1. Reported Kerr coefficient n_2 values for 1-decanol.

Reference	Wavelength (nm)	Method	n_2 (m^2/W)
This work	785	Closed-aperture Z-scan	1.87×10^{-20}
Our previous work [33]	785	Z-scan	6.8×10^{-20}
Ho et al. [43]	1064	ps OKE	10.9×10^{-20}
Kuzyk & Dirk [36]	1064	ns OKE [44][a]	622×10^{-20}

[a]Optically induced Kerr constant B_0 reported in Ref. [44] and converted to n_2 in Ref. [36].

Figure 3 shows the high-intensity, SC regime where we observe an intensity dependent thermal effect consistent with the generation of a spatial optical soliton [46]. In this regime, the data do not follow the Z-scan shape exhibited in Fig. 2(a). Because the Z-scan technique breaks down in this regime, we do not use it to calculate the nonlinear index of the medium. The breakdown of the fit begins at $>1 \times 10^{15}$ W/m^2 and becomes more apparent $>2 \times 10^{15}$ W/m^2. We argue that multi-photon absorption is not responsible for the disagreement with the Z-scan fit because we do not measure additional power loss through the cuvette at these high intensities.

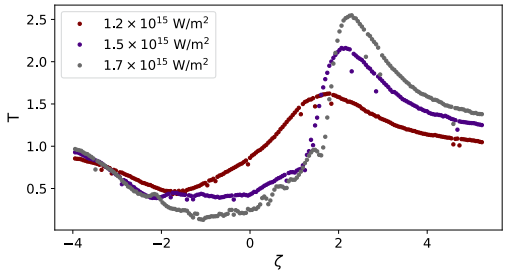

Fig. 3. High-intensity Z-scans. In this regime, the Z-scan fit (Eq. (1)) breaks down due intensity-dependent thermal effects. At these intensities, we observe supercontinuum generation near $\zeta = 0$.

Optics EXPRESS

3.2. Spectrum vs. axial position

Figure 4(a) illustrates the intensity of the spectrum as a function of wavelength and cuvette position. As the 1-decanol approaches the focus, the spectrum undergoes significant spectral broadening, creating a SC which is stable until the 1-decanol passes out of the focus and returns to its initial bandwidth. The WLC spans from approximately 450 nm to 950 nm, and the significant extension on the blue side of the spectrum at $\zeta = -2$ can likely be attributed to self-steepening [47], and we note that the upper limit of our spectrometer is approximately 1000 nm due to the silicon detector, thus limiting our measurements from extending further into the infrared. We also previously measured the absorption spectrum of 1-decanol and found that it is weakly absorbing beyond 900 nm [34].

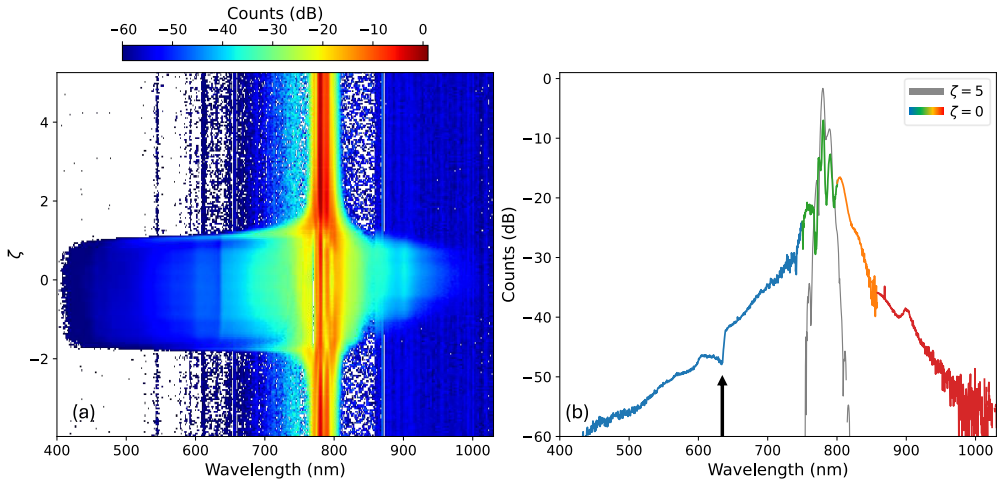

Fig. 4. (a) As the cuvette passes through the focus ($\zeta = 0$), the spectrum rapidly broadens into a white light continuum. (b) A lineout of the spectrum at the focus ($\zeta = 0$) and far from the focus ($\zeta = 5$). Colours indicate the bandwidth of each optical filter used in the measurement; arrow indicates position of the Raman loss.

Figure 4(b) shows lineouts contrasting the initial spectrum ($\zeta = 5$) to the SC ($\zeta = 0$). The peak intensity of the beam at the focus is estimated to be 3×10^{15} W/m^2. The difference in energy between 785 nm and 636 nm corresponds to a Raman shift of -2984 cm^{-1}, which lies within the broad Raman response of 1-decanol centered at 2900 cm^{-1} [48], indicating Raman loss caused by the pump (black arrow) [49–52]. Apart from this localized feature, Raman effects do not dominate the supercontinuum generation process. Since we operate in the normal dispersion regime for 1-decanol, we do not generate the strong Raman frequency shift that is characteristic of anomalous-dispersion soliton dynamics. Furthermore, our femtosecond pump pulse is too short for efficient stimulated Raman cascade effects on the red side of the pump [53]. Therefore, we argue that the mechanism for supercontinuum generation is dominated by self-phase modulation and self-steepening. However at the high intensities shown in Fig. 3, additional nonlinear effects come into play and absorption, thermal lensing, self-focusing, and diffraction allow for extending the high-intensity interaction length, enabling more efficient SC generation via the generation of a spatial optical soliton [46,54].

3.3. Spectrum vs. radial angle

The radial distribution of the spectrum, as shown in Fig. 5, is such that all wavelengths in the supercontinuum are present near the center of the beam. However, while the visible wavelengths

Optics EXPRESS

remain present at greater radial distances, the infrared components do not. Furthermore, we do not observe significant spectral peak shifts off-axis.

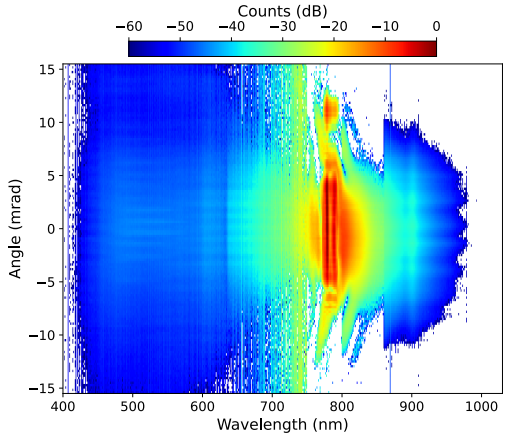

Fig. 5. The broad spectrum produced in 1-decanol as a function of radial angle from the center of the output beam. The visible portion exhibits a large divergence, indicative of the tight spatial confinement in the supercontinuum generation process.

The visible portion of the spectrum is relatively uniform and not significantly radially dependent over this divergence. This angle-wavelength distribution exhibits a different pattern than the X-wave amplification exhibited from four-wave mixing [55].

3.4. *Temporal stability of the spectrum*

Laser power fluctuations and material degradation would cause instability in the edges of the supercontinuum. As shown in Fig. 6, we measured the temporal stability of the SC over the main portion of the spectrum for 30 minutes. A benchmark of stability for SC spectra in liquids is found in [16] where the authors report a spectrum stable for over 70 hours using CS_2 in a liquid-core fiber. Because of the high boiling point of 1-decanol, we observe little evaporation of the sample after several weeks of repeated use and we expect similar longevity in our sample.

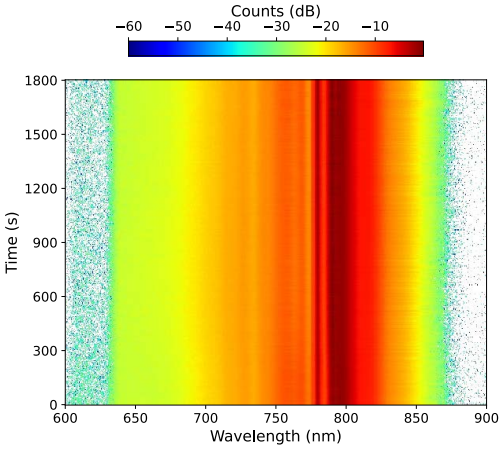

Fig. 6. The temporal stability of the most intense portion of the spectrum over 30 minutes, demonstrating little variation in the supercontinuum.

Optics EXPRESS

4. Conclusion

We show that it is possible to generate a broad white light continuum in 1-decanol that spans from 450 to 950 nm. Although the nonlinear Kerr coefficient is modest, we find that the higher-order nonlinearities significantly contribute to the measured phase shift. Not only is 1-decanol a much safer alternative to commonly used liquids such as chloroform ($CHCl_3$), carbon disulfide (CS_2), toluene (C_7H_8), and benzene (C_6H_6), but it demonstrates a nonlinear index on par with these liquids at high intensities. Additionally, we find that the supercontinuum is stable for extended periods of time, enabling prolonged study of strong-field physics. We expect that the comparable nonlinearity of 1-decanol to more toxic liquids makes it an attractive alternative for future nonlinear optics applications such as Kerr-instability amplification.

4.1. Data availability

(1) TJ Hammond, "Data to replicate supercontinuum generation in 1-decanol," figshare (2014), https://doi.org/10.5683/SP3/4HLCO9.

Funding. This work was supported by the Natural Sciences Research Council of Canada (RGPIN-2019-06877); Mitacs Globalink Research Internship; Canada Foundation for Innovation (John R. Evans Leaders Fund, project number 38804); the Ontario Research Fund, and the University of Windsor. The authors also acknowledge financial support from Canada Research Chair CRC2023-00089.

Acknowledgment. We want to thank Aldo DiCarlo for his technical assistance and Jill Crossman for her support.

Disclosures. "The authors declare no conflicts of interest."

Data availability. Data availability. Data underlying the results presented in this paper are available in Ref. [35].

References

1. Y. Liu, H. Tu, and S. A. Boppart, "Wave-breaking-extended fiber supercontinuum generation for high compression ratio transform-limited pulse compression," Opt. Lett. **37**(1), 1 (2012).
2. T. Gaumnitz, A. Jain, Y. Pertot, *et al.*, "Streaking of 43-attosecond soft-x-ray pulses generated by a passively CEP-stable mid-infrared driver," Opt. Express **25**(22), 27506 (2017).
3. F. Krausz and M. Ivanov, "Attosecond physics," Rev. Mod. Phys. **81**(1), 163–234 (2009).
4. T. J. Hammond, S. Monchocé, C. Zhang, *et al.*, "Integrating solids and gases for attosecond pulse generation," Nat. Photonics **11**(9), 594–599 (2017).
5. E. Goulielmakis, M. Schultze, M. Hofstetter, *et al.*, "Single-cycle nonlinear optics," Science **320**(5883), 1614–1617 (2008).
6. M. T. Hassan, T. T. Luu, A. Moulet, *et al.*, "Optical attosecond pulses and tracking the nonlinear response of bound electrons," Nature **530**(7588), 66–70 (2016).
7. S.-F. Gao, Y.-Y. Wang, F. Belli, *et al.*, "From raman frequency combs to supercontinuum generation in nitrogen-filled hollow-core anti-resonant fiber," Laser Photonics Rev. **16**(4), 2100426 (2022).
8. A. I. Adamu, M. S. Habib, C. R. Petersen, *et al.*, "Deep-uv to mid-ir supercontinuum generation driven by mid-ir ultrashort pulses in a gas-filled hollow-core fiber," Sci. Rep. **9**(1), 4446 (2019).
9. K. Y. Kim, A. J. Taylor, J. H. Glownia, *et al.*, "Coherent control of terahertz supercontinuum generation in ultrafast laser-gas interactions," Nat. Photonics **2**(10), 605–609 (2008).
10. A. M. Heidt, A. Hartung, G. W. Bosman, *et al.*, "Coherent octave spanning near-infrared and visible supercontinuum generation in all-normal dispersion photonic crystal fibers," Opt. Express **19**(4), 3775 (2011).
11. R. Grigutis, G. Tamošauskas, V. Jukna, *et al.*, "Supercontinuum generation and optical damage of sapphire and YAG at high repetition rates," Opt. Lett. **45**(16), 4507 (2020).
12. V. Marčiulionyté, V. Jukna, G. Tamošauskas, *et al.*, "High repetition rate green-pumped supercontinuum generation in calcium fluoride," Sci. Rep. **11**(1), 15019 (2021).
13. L. C. Van, V. T. Hoang, V. C. Long, *et al.*, "Supercontinuum generation in benzene-filled hollow-core fibers," Opt. Eng. **60**(11), 116109 (2021).
14. T. N. Thi, D. H. Trong, B. T. L. Tran, *et al.*, "Optimization of optical properties of toluene-core photonic crystal fibers with circle lattice for supercontinuum generation," J. Opt. (2022).
15. C. Manzoni and G. Cerullo, "Design criteria for ultrafast optical parametric amplifiers," J. Opt. **18**(10), 103501 (2016).
16. K. Schaarschmidt, H. Xuan, J. Kobelke, *et al.*, "Long-term stable supercontinuum generation and watt-level transmission in liquid-core optical fibers," Opt. Lett. **44**(9), 2236–2239 (2019).
17. P. Kumar, K. F. Fiaboe, and J. S. Roy, "Design of nonlinear photonic crystal fibers with ultra-flattened zero dispersion for supercontinuum generation," ETRI J. **42**(2), 282–291 (2020).
18. W. M. Haynes, *CRC Handbook of Chemistry and Physics 95th Edition* (CRC Press, 2014).

Optics EXPRESS

19. C. V. Lanh, V. T. Hoang, V. C. Long, *et al.*, "Optimization of optical properties of photonic crystal fibers infiltrated with chloroform for supercontinuum generation," Laser Phys. **29**(7), 075107 (2019).
20. C. Wang, G. Feng, W. Li, *et al.*, "Highly coherent supercontinuum generation in cs2 -infiltrated single-core optical fiber," J. Opt. **21**(10), 105501 (2019).
21. C. Lionte, "Lethal complications after poisoning with chloroform - case report and literature review," Hum Exp. Toxicol. **29**(7), 615–622 (2010).
22. Y. Yan, C. Wang, Z. Zheng, *et al.*, "Renal injury following long-term exposure to carbon disulfide: analysis of a case series," BMC Nephrol. **20**(1), 377 (2019).
23. S. L. Cruz, M. T. Rivera-García, and J. J. Woodward, "Review of toluene actions: Clinical evidence animal studies, and molecular targets," J. Drug Alcohol. Res. **3**, 1–8 (2014).
24. R. Snyder, G. Witz, and B. D. Goldstein, "The toxicology of benzene," Environ Health Perspect **100**, 293–306 (1993).
25. H. Greim, *Forschungsgemeinschaft, Significance Use and Derivation of MAK Values* (Wiley Online Library, 2015).
26. A. Hartwig, *MAK value documentation* (Wiley Online Library, 2011).
27. D. Stevenz, *Carbon disulfide* (Wiley Online Library, 2002).
28. H. Greim, *Chloroform* (Wiley, 2012).
29. Angerer and Gundel, *Benzene and Alkylbenzenes* (Wiley Online Library, 2002).
30. H. Greim, *Toluene* (Wiley, 2012).
31. N. O. of Response and Restoration, "Carbon disulfide,", (2022).
32. D. Ambrose and C. Sprake, "Thermodynamic properties of organic oxygen compounds xxv. vapour pressures and normal boiling temperatures of aliphatic alcohols," J. Chem. Thermodyn **2**(5), 631–645 (1970).
33. J. A. Stephen, C. J. Arachchige, and T. J. Hammond, "Spectral broadening for pulse compression using liquid alcohols," J. Phys. B **55**(15), 155402 (2022).
34. N. G. Drouillard and T. J. Hammond, "Measurement of dispersion and index of refraction of 1-decanol with spectrally resolved white light interferometry," Opt. Express (2022).
35. T. J. Hammond, "Data to replicate supercontinuum generation in 1-decanol," (2025). Dataset.
36. M. G. Kuzyk and C. W. Dirk, eds., *Characterization Techniques and Tabulations for Organic Nonlinear Optical Materials*, vol. 60 of *Optical Engineering* (Marcel Dekker, New York, 1998).
37. G. Boudebs, S. Cherukulappurath, H. Leblond, *et al.*, "Experimental and theoretical study of higher-order nonlinearities in chalcogenide glasses," Opt. Commun. **219**(1-6), 427–433 (2003).
38. J. Ortega, "Densities and refractive indices of pure alcohols as a function of temperature," J. Chem. Eng. Data **27**(3), 312–317 (1982).
39. S. Couris, M. Renard, O. Faucher, *et al.*, "An experimental investigation of the nonlinear refractive index (n2) of carbon disulfide and toluene by spectral shearing interferometry and z-scan techniques," Chem. Phys. Lett. **369**(3-4), 318–324 (2003).
40. R. A. Ganeev, A. I. Ryasnyanskiĭ, and H. Kuroda, "Nonlinear optical characteristics of carbon disulfide," Opt. Spectrosc. **100**(1), 108–118 (2006).
41. D. G. Kong, Q. Chang, H. A. Ye, *et al.*, "The fifth-order nonlinearity of cs2," J. Phys. B **42**(6), 065401 (2009).
42. V. Besse, H. Leblond, and G. Boudebs, "Filamentation of light in carbon disulfide," Phys. Rev. A **89**(4), 043840 (2014).
43. P. P. Ho and R. R. Alfano, "Optical kerr effect in liquids," Phys. Rev. A **20**(5), 2170–2187 (1979).
44. N. Harrison and B. Jennings, "Optical kerr-effect measurement for a series of alcohols," J. Appl. Phys. **73**(12), 8076–8080 (1993).
45. D. Milam, "Review and assessment of measured values of the nonlinear refractive-index coefficient of fused silica," Appl. Opt. **37**(3), 546–550 (1998).
46. E. L. Falc ao Filho, C. B. de Araújo, G. Boudebs, *et al.*, "Robust two-dimensional spatial solitons in liquid carbon disulfide," Phys. Rev. Lett. **110**(1), 013901 (2013).
47. V. Kandidov, O. Kosareva, I. Golubtsov, *et al.*, "Self-transformation of a powerful femtosecond laser pulse into a white-light laser pulse in bulk optical media (or supercontinuum generation)," Appl. Phys. B **77**(2-3), 149–165 (2003).
48. D. Carrizo, V. Muñoz-Iglesias, M. T. Fernández-Sampedro, *et al.*, "Detection of potential lipid biomarkers in oxidative environments by raman spectroscopy and implications for the exomars 2020-raman laser spectrometer instrument performance," Astrobiology **20**(3), 405–414 (2020).
49. J. Yang and G. Mu, "Multi-dimensional observation of white-light filaments generated by femtosecond laser pulses in condensed medium," Opt. Express **15**(8), 4943 (2007).
50. C. Santhosh, A. K. Dharmadhikari, J. A. Dharmadhikari, *et al.*, "Supercontinuum generation in macromolecular media," Appl. Phys. B **99**(3), 427–432 (2010).
51. S. Sreeja, C. Leela, V. R. Kumar, *et al.*, "Dynamics of tightly focused femtosecond laser pulses in water," Laser Phys. **23**(10), 106002 (2013).
52. N. G. Drouillard and T. J. Hammond, "Stimulated raman spectroscopy using a tunable visible broadband probe pulse generated by kerr instability amplification," Appl. Spectrosc. **80**(1), 83–90 (2026).
53. J. Dudley, G. Genty, and S. Coen, "Supercontinuum generation in photonic crystal fiber," Rev. Mod. Phys. **78**(4), 1135–1184 (2006).
54. J. E. Q. Bautista, M. L. da Silva-Neta, C. L. A. V. Campos, *et al.*, "Thermal and non-thermal intensity dependent optical nonlinearities in ethanol at 800 nm, 1480 nm, and 1560 nm," J. Opt. Soc. Am. B **38**(4), 1104–1111 (2021).

Optics EXPRESS

55. D. Faccio, M. A. Porras, A. Dubietis, *et al.*, "Conical emission, pulse splitting, and x-wave parametric amplification in nonlinear dynamics of ultrashort light pulses," Phys. Rev. Lett. **96**(19), 193901 (2006).